IGFBP2 induces podocyte apoptosis promoted by mitochondrial damage via integrin α5/FAK in diabetic kidney disease

Xiaochen Wang[1] · Yifan Zhang[1] · Kun Chi[1] · Yuwei Ji[1] · Keying Zhang[1] · Ping Li[1] · Zhangning Fu[1] · Xu Wang[1] · Shaoyuan Cui[1] · Wanjun Shen[1] · Guangyan Cai[1] · Xiangmei Chen[1] · Hanyu Zhu[1] · Quan Hong[1]

Abstract

Podocyte apoptosis or loss is the pivotal pathological characteristic of diabetic kidney disease (DKD). Insulin-like growth factor-binding protein 2 (IGFBP2) have a proinflammatory and proapoptotic effect on diseases. Previous studies have shown that serum IGFBP2 level significantly increased in DKD patients, but the precise mechanisms remain unclear. Here, we found that IGFBP2 levels obviously increased under a diabetic state and high glucose stimuli. Deficiency of IGFBP2 attenuated the urine protein, renal pathological injury and glomeruli hypertrophy of DKD mice induced by STZ, and knockdown or deletion of IGFBP2 alleviated podocytes apoptosis induced by high concentration of glucose or in DKD mouse. Furthermore, IGFBP2 facilitated apoptosis, which was characterized by increase in inflammation and oxidative stress, by binding with integrin α5 (ITGA5) of podocytes, and then activating the phosphorylation of focal adhesion kinase (FAK)-mediated mitochondrial injury, including membrane potential decreasing, ROS production increasing. Moreover, ITGA5 knockdown or FAK inhibition attenuated the podocyte apoptosis caused by high glucose or IGFBP2 overexpression. Taken together, these findings unveiled the insight mechanism that IGFBP2 increased podocyte apoptosis by mitochondrial injury via ITGA5/FAK phosphorylation pathway in DKD progression, and provided the potential therapeutic strategies for diabetic kidney disease.

Keywords IGFBP2 · Mitochondrial damage · FAK · ROS · Diabetic kidney disease

Introduction

Diabetic kidney disease (DKD) is renal structure and function abnormalities due to chronic microvascular diabetes complications, and accounts for 50% of new end-stage renal disease (ESRD) [1]. At present, DKD drugs are mainly divided into RAS blockers and SGLT2 inhibitors [2], which can partially improve the condition of patients, but there are still patients who continue to develop disease. New

therapeutic targets are expected to improve current insufficient regimen and prevent DKD progress to ESRD. DKD is composed of several glomerular changes including glomerular basement membrane (GBM) thickening, foot process effacement and podocyte detachment [3].

Podocyte, a type of highly terminally differentiated epithelial cells, which is essential for maintain the glomerular structure and function [4]. Podocyte apoptosis or loss disrupts the integrity of the glomerular filtration membrane and leads to proteinuria in glomerular diseases [4]. Attention should be given to changes that is both podocyte foot process effacement and podocyte number reduction the early stage of DKD [5–7]. Diabetes-induced podocyte dysfunction is associated with inflammation, mitochondrial injury and subsequent increase in cellular oxidative stress, which contribute to podocyte apoptosis reported by many researches [8–10]. Therefore, further discussing the mechanism of podocyte injury can be expected to prevent DKD.

Insulin growth factor binding protein family (IGFBPs), as a cluster of insulin-like growth factor ligand proteins, had been discovered association with diabetes and involving in the

---

Xiaochen Wang, Yifan Zhang, and Kun Chi contributed equally to this work.

✉ Hanyu Zhu
hanyuzhu301@126.com

✉ Quan Hong
hongquan@301hospital.com.cn

[1] Department of Nephrology, First Medical Center of Chinese PLA General Hospital, State Key Laboratory of Kidney Diseases, National Clinical Research Center for Kidney Diseases, Beijing Key Laboratory of Kidney Diseases Research, Beijing 100853, China

physiological processes of several kidney diseases such as glomerulosclerosis [11] and acute kidney injury [12]. IGFBP-1 [13], 3 [14], 4 [15], 5 [16] are associated with the development of DKD, and our pervious study shows that IGFBP-5 plays a pro-inflammatory role in the pathogenesis of DKD through glycolysis in endothelial cells [16]. IGF-2 is a secreted protein with a molecular weight of about 34.8kD [17], which is involved in glucose metabolism [18], cell inflammation [19, 20], cell mobility [21] and cell death [20]. Single cell sequencing of adult kidney showed that IGFBP2 was mainly expressed in podocytes. High expression of IGFBP2 in patients with type 2 diabetes are associated with decreased estimated glomerular filtration rate (eGFR) and increased proteinuria as the disease progresses [22]. Thus, IGFBP2 has an important role that was also involved to the pathogenesis of podocyte injury in DKD.

Unlike the IGF dependent pathway, IGFBP2 regulates cell process through the IGF independent pathway by activating Focal adhesion kinase (FAK) phosphorylation with integrin signaling [23]. FAK is a non-receptor tyrosine kinase that is a key mediator of integrin signaling between different cellular functions [24]. FAK knockout or blocking is reported to alleviate podocyte damage induced by lipopolysaccharide

and anti-GBM nephropathy models [25]. Other study also has shown a relationship between integrin/FAK and oxidative stress [26]. These findings strongly suggest that IGFBP2 promote the development of diabetic complications. However, the specific mechanism of IGFBP2 on podocyte in this context of DKD are not well understood. Above all, we hypothesized that IGFBP2 activated podocyte apoptosis by regulating mitochondria-induced oxidative stress. Therefore, in this study, we aimed to clarify the role of IGFBP2 in diabetic renal podocytes and search for potential intervention targets to DKD prevention and treatment.

Methods and material

Urine sample

Morning urine was collected from 6 type 2 diabetic mellitus and 9 diabetic kidney disease of the Chinese PLA General Hospital. The inclusion criteria for 9 patients diabetic kidney disease (male 5 and female 4) were as follows: age of over 18 with kidney biopsy support; informed consent. The.
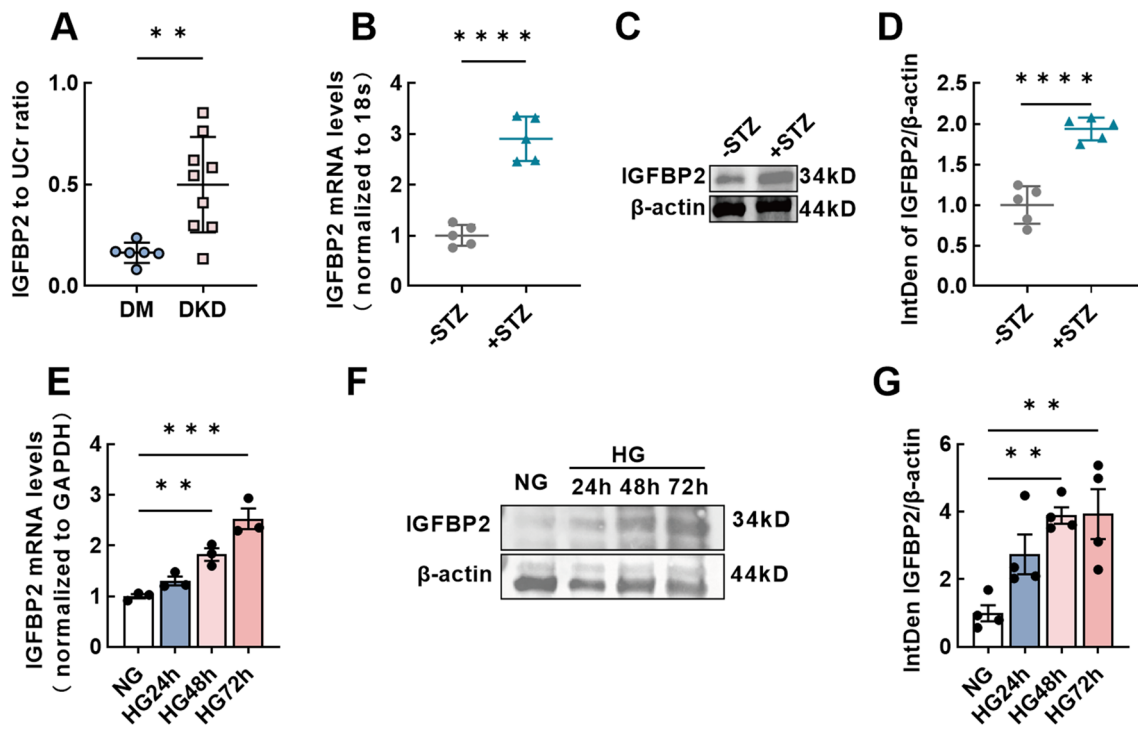

Fig. 1 IGFBP2 is increased in DKD patients, mouse and podocyte. **A** ELISA analysis of urinary IGFBP2 level from DM(n=6) and DKD(n=9) patients shown as mean±SD. **B** IGFBP2 mRNA was analyzed by RT-qPCR in renal tissue of mice with or without STZ shown as mean±SD. n=5. **C, D** Representative western blot and matched densitometric quantification of IGFBP2 level in renal tissue of mice with or without STZ shown as mean±SD. n=5. **E** RT-qPCR analysis of IGFBP2 mRNA expression of podocyte with normal glucose (NG) and high glucose (HG) at different time points shown as mean±SEM n=3. **F, G** Representative western blot analysis and densitometric quantification of IGFBP2 protein level of podocyte with normal glucose (NG) and high glucose (HG) at different time points shown as mean±SEM. n=4. $^{**}P<0.01$, $^{***}P<0.001$, $^{****}P<0.0001$

Fig. 2 IGFBP2 deletion mitigates STZ-induced diabetic injury. **A** Schematic design of study. IGFBP2^{wt} and IGFBP2^{null} mice were injected with STZ or citrate buffer and were monitored biweekly starting at 8 weeks of age. All mice were euthanized at 24 weeks of age. **B**, **C** Measurement of blood glucose and body weight in -STZ and +STZ mice from 8 to 24 weeks of age. **D** Ratio of kidney/body weight at the day of euthanization. **E** Urine albumin-to-creatinine ratio of spot urine over time. **F** Representative images of renal tissue stained with periodic acid-Schiff. Original magnification ×400, Scale bar = 50 µm. **G**, **H** Quantification of the fraction of glomerular volume and mesangial area per mouse. All data shown as mean ± SD, n = 6. **$P < 0.01$, ***$P < 0.001$; #$P < 0.05$, ##$P < 0.01$
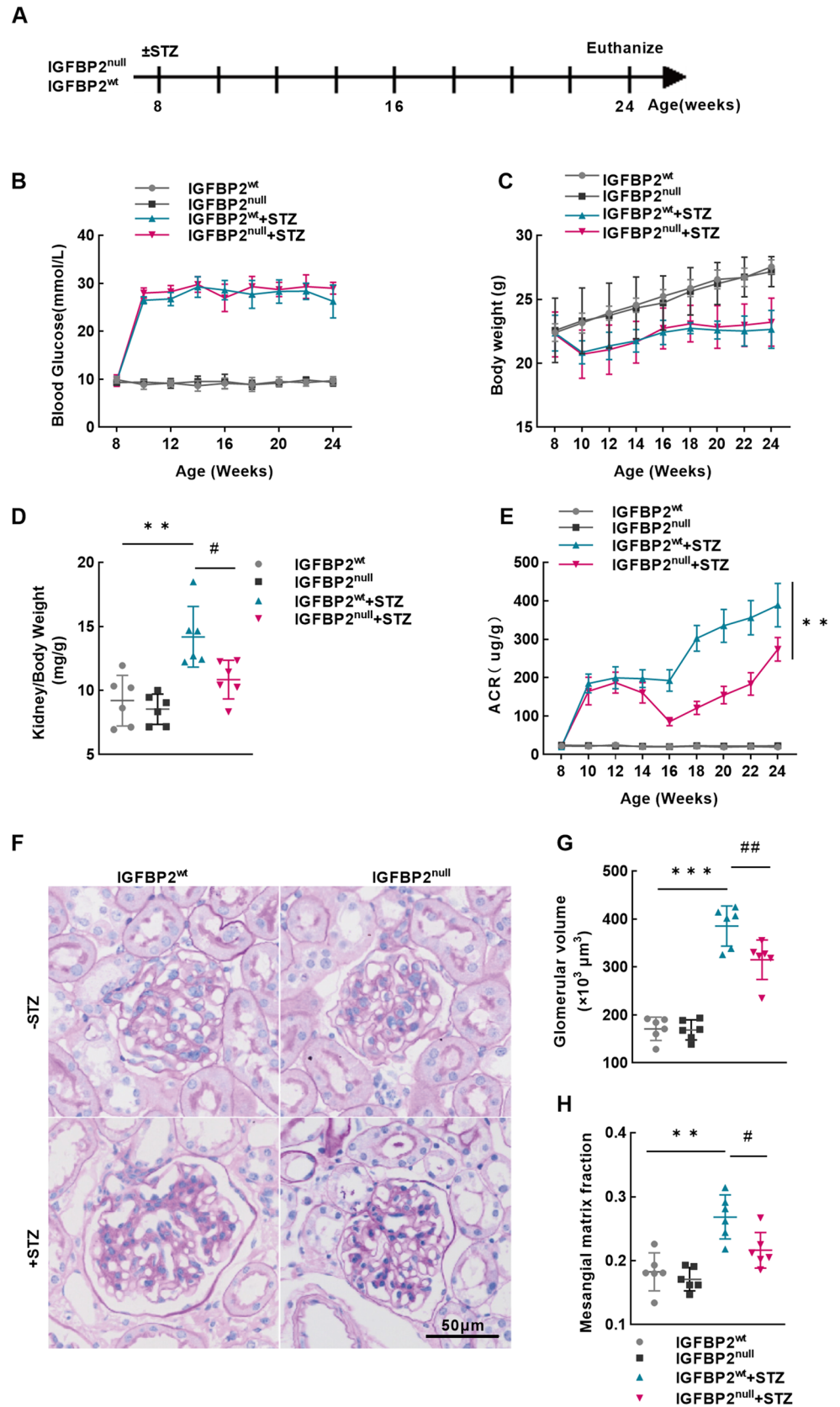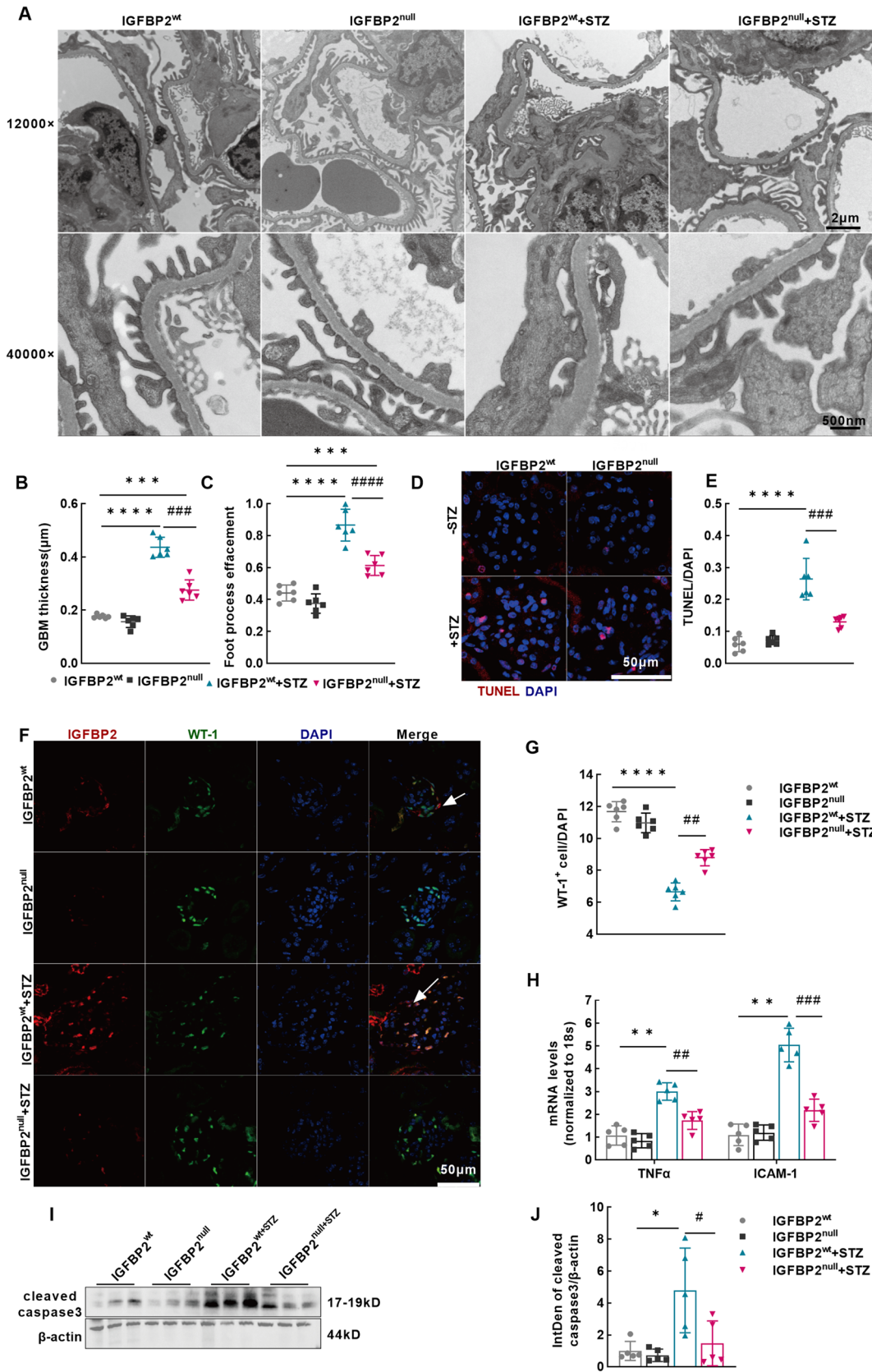
◀**Fig. 3** IGFBP2 deletion attenuate STZ-induced podocyte injury. **A** Representative image of ultrastructural changes in glomerular basement membrane and podocyte morphology performed by electron microscopy shown in IGFBP2^{wt} and IGFBP2^{null} mice. Top panel: original magnification ×12,000, Scale bar = 2 µm; bottom panel: original magnification ×40,000, Scale bar = 500 nm. n = 6. **B**, **C** Quantification of glomerular basement membrane thickness and podocyte effacement. n = 6. **D** Representative images showing TUNEL(Red) staining. DAPI(Blue). Scale bars = 50 µm. **E** Quantification of TUNEL/DAPI ratio in IGFBP2^{wt} and IGFBP2^{null} mice. n = 6. **F** Representative fluorescence microscopy demonstrating the glomerular distribution of IGFBP2(Red) and WT-1(Green). Nuclei stained with DAPI(Blue). Arrows indicate cytoplasmic clusters of IGFBP2. Scale bars = 50 µm. n = 6. **G** Quantification of WT-1$^+$ cells in diabetic and non-diabetic IGFBP2^{wt} and IGFBP2^{null} mice. n = 6. **H** mRNA levels of TNF-α and ICAM-1 detected by RT-qPCR analysis. n = 5. **I**, **J** Representative pictures and quantification of cleaved caspase3 detected by western blotting. n = 5. All data shown as mean ± SD. *$P < 0.05$, **$P < 0.01$, ***$P < 0.001$, ****$P < 0.0001$; #$P < 0.05$, ##$P < 0.01$, ###$P < 0.001$, ####$P < 0.0001$

exclusion criteria were as follow: incomplete medical history; presence of other types of secondary renal disease and hereditary kidney disease; and combined urinary tract infection, cancer, or pregnancy. Two qualified pathologists rigorously diagnosed slides from kidney biopsy. The informed consent form had to be voluntarily signed by all participants before enrollment. Morning urine samples were obtained from 6 to 9 am, placed on ice and centrifuged at 4500 g at 4 °C for 45 min. 1 ml of supernatant was pipetted into a new frozen pipe and Protease cocktail inhibitor (Sigma-Aldrich, St. Louis, MO) was added to protect urine protein at a dilution of 1/1000 before storage at −80 °C. The participant information is given in Table S1. All experiments were conducted in accordance with the Declaration of Helsinki. The study protocol was approved by the Ethics Committee of the Chinese PLA General Hospital (No. S2017-133-01).

IGFBP2 ELISA

Human urinary IGFBP2 levels were quantified using IGFBP2 ELISA. (PeproTech), following the manufacturer's instructions. 100 µl urine supernatant was added to measure IGFBP2 concentration. IGFBP2 levels normalized to urine creatinine was used to compare between patients with diabetes mellitus and DKD.

Mouse model

The IGFBP2 null mouse with FVB background was engineered by Cygen using CRISPR-Cas9 technique, ensuring precise gene targeting. Mice were maintained under specific pathogen-free conditions, with a controlled temperature of 25℃ and a standard diet. All studies involving animals were approved by the Ethics Committee of PLA General

Hospital. PCR genotyping was performed using specific primers (sequences provided in Table S2) under defined conditions shown in Table S3, targeting the IGFBP2 gene mutation. At 8 weeks of age, the male IGFBP2 null and wild type (WT) FVB mice were intraperitoneal administered with streptozotocin (STZ, S0103, Sigma, USA) dissolved in 0.1 M citrate buffer at 50 mg/kg after a 4-h fast to standardize metabolic condition for 5 consecutive days. Blood glucose was measured at 7 days after the last injection. The diabetic model was considered successful if mice exhibited a random blood glucose level > 16.7 mM over consecutive measurements. Body weight, blood glucose and random spot urine were monitored every two weeks. All mice were euthanized at 16 weeks after STZ or citrate buffer injection.

Measurements of urinary albumin and creatinine

Mouse albumin ELISA kit (Bethyl Laboratories, Montgomery, TX, USA) was performed to measure the urine albumin concentration. Creatinine colorimetric assay kit (Cayman, MI, USA) was performed to detect the urine creatinine levels, following the manufacture's instruction.

Kidney histology

Kidney samples were fixed in 10% formalin, embedded in paraffin, and sectioned to 2 µm thickness. The sections were stained with periodic acid–Schiff (PAS) to analyze the glomerular area and mesangial matrix expansion as previously described [10]. 400× magnification of light microscope was performed to revel and obtain the histopathological image (Olympus, Tokyo, Japan). The mean glomerular cross-sectional area by light microscopy was used to calculate the mean glomerular volume, as previously described [10]. The foot process effacement and the width of glomerular basement membrane were obtained from transmission electron microscope (Hitachi H7650 Microscope, Japan) and measured using ImageJ software, as previously described [10, 27].

Immunofluorescent staining

IGFBP2 and wilms tumor 1 (WT-1) were examined in 4 µm frozen sections of mouse renal tissues, which then is blocked by skinned milk at 1 h and incubated with primary antibody overnight at 4 °C, followed by incubation with fluorescent secondary antibodies at 37 °C for 2 h in the dark. The sections were counterstained and sealed DAPI dye and detected by confocal fluorescence microscopy (Olympus, Japan).
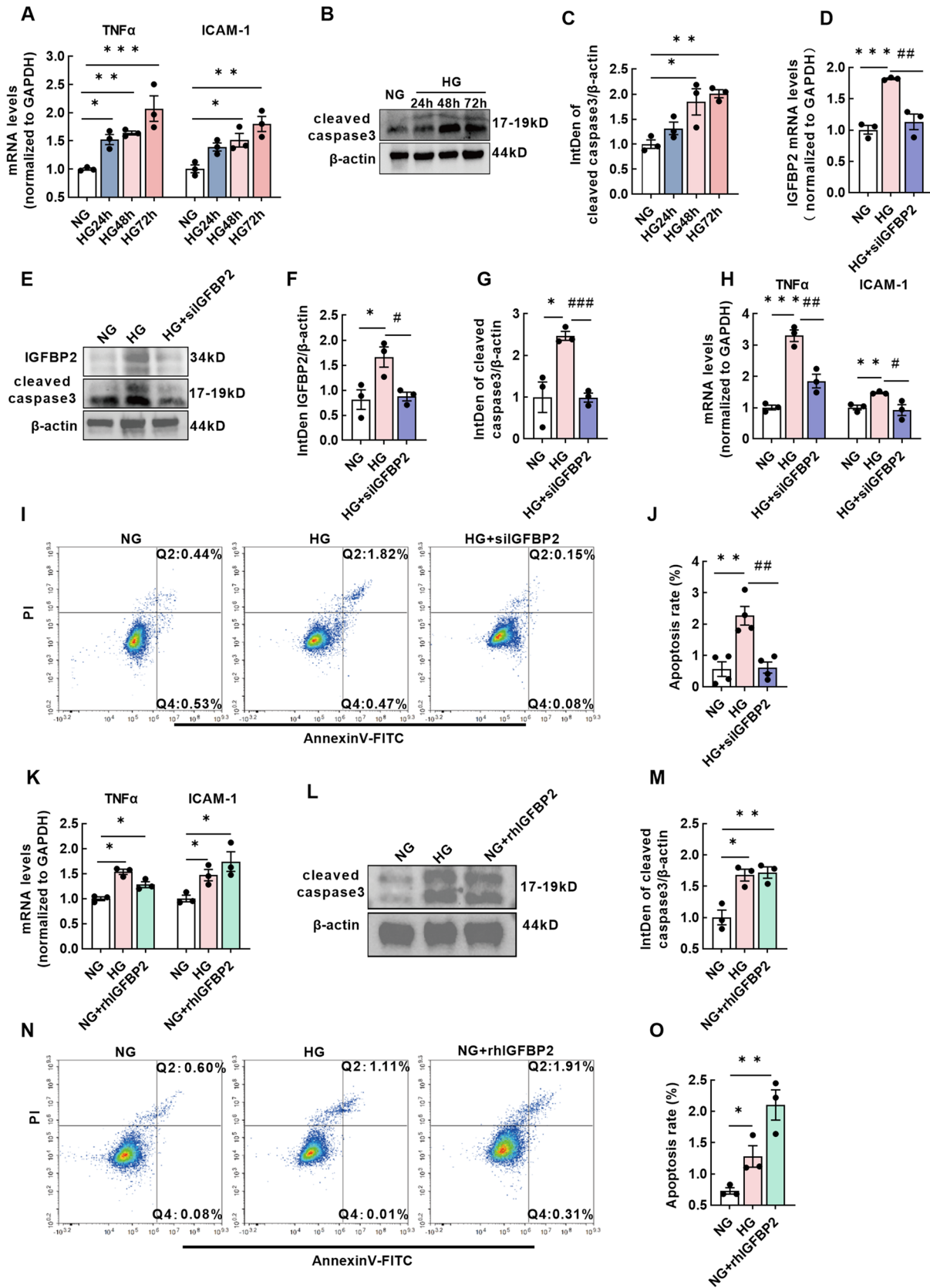
◀ **Fig. 4** IGFBP2 regulates the podocyte inflammation and apoptosis. **A** RT-qPCR analysis of TNF-α and ICAM-1 mRNA expression on podocyte with NG or HG treatment over time. n = 3. **B**, **C** Western blot analysis and densitometric quantification of cleaved caspase3 protein level over time. n = 3. **D** Transfection efficiency of IGFBP2 in podocyte interfered with siIGFBP2 under HG condition performed by RT-qPCR analysis. n = 3. **E**, **F**, **G** Representative image and quantification of IGFBP2 and cleaved caspase3 protein levels performed by western blot on podocyte under NG, HG and HG with siIGFBP2 conditions. n = 3. **H** RT-qPCR analysis of TNF-α and ICAM-1 mRNA expression on podocyte under NG, HG and HG with siIGFBP2 conditions. n = 3. **I-J** Representative graphs and quantification of apoptosis rate on podocyte performed by flow cytometry under NG, HG and HG with siIGFBP2 conditions. n = 4. **K** RT-qPCR analysis of TNF-α and ICAM-1 mRNA expression on podocyte NG, HG and NG with 125 ng/ml rhIGFBP2 treatments. n = 3. **L-M** Representative image and quantification of cleaved caspase3 protein levels performed by western blot on podocyte under NG, HG and NG with 125 ng/ml rhIGFBP2 treatments. n = 3. **N–O** Representative graph and quantification of apoptosis rate on podocyte performed by flow cytometry under NG, HG and NG with 125 ng/ml rhIGFBP2 treatments. n = 3. All data shown as mean ± SEM. *$P < 0.05$, **$P < 0.01$, ***$P < 0.001$; #$P < 0.05$, ##$P < 0.01$, ###$P < 0.001$

TUNEL assay

The Rapid One Step TUNEL Apoptosis Assay Kit (Key-GEN) was used to detect apoptotic cells on formalin-fixed and paraffin-embedded sections following the manufacturer's instructions. KeyFlour555-conjugated streptavidin was used to detect the apoptotic cells, and sections were then mounted with DAPI.

Cell culture and pharmacologic compounds

The human podocyte cell line was obtained from Dr. Moin Saleem (University of Bristol, UK) and cultured in RPMI 1640 (Corning) supplemented with 10% FBS, 1% penicillin/streptomycin at a humidified incubator with 5% CO2 in 33 °C under growth-permissive (GP) conditions or in 37 °C growth-restrictive (GR) conditions. After 7 to 14-day differentiation, podocytes were starved with serum-free medium for 6 h, followed by normal glucose (5 mM) or high glucose (30 mM) supplement. Recombination human IGFBP2(350-06B.USA) was purchased from PeproTech and used as an extracellular IGFBP2 stimuli at 125 ng/ml. PND1186 (1061353–68, MedChemExpress, China) was used as a FAK inhibitor at 0.4 μM for the experiment.

IGFBP2 plasmid and siRNA transfection

Podocyte were transfected with a pIRES2-EGFP expression vector encoding IGFBP2 cDNA (IGFBP2^OV) using the Lipofectamine 3000 reagent (Invitrogen). Plasmid DNA (1 μg) with 2 μl P3000 reagent and 125 μl Opti-MEM medium, as well as 3 μl of Lipofectamine 3000 and 125μL Opti-MEM medium were added to ∼ 70% adherent cells in a 6-well plate and incubated within serum-free medium for 6 h at 37°C incubator. Small interfering RNA targeting human IGFBP2, and ITGA5 were purchased from GenePharma (Shanghai, China). Sequences as listed in the Table S4. The siRNA transfections for podocyte were performed using Lipofectamine 3000 reagent and Opti-MEM medium following the manufacturer's instructions. After 48 h transfection, RNA and protein were collected.

RNA extraction and real time PCR

Total RNA was extracted from cells or kidney tissue using TRIzol reagent (Invitrogen, Grand Island, NY). 2 μg of RNA was used to synthesize complementary DNAs (cDNAs) with the PrimeScript IV 1st strand cDNA Synthesis System (6215A, TaKaRa, Japan). Real-time PCR was performed with PowerUp™ SYBR™ Green mix (A25742, Applied Biosystems, USA), and the relative gene expression was determined on a QuantStudio 5 quantitative PCR machine (A28140, ABI Biosystems). The 2^-ΔΔCt method was used to determine the comparative mRNA level, which were normalized to the expression of glyceraldehyde-3-phosphate dehydrogenase (GAPDH) or 18S as reference genes. BGI company (Shenzhen, China) synthesized the gene primers shown in Table S5.

Western blotting

Cells and tissue were lysed in RIPA buffer with phenylmethanesulfonyl fluoride (PMSF) (Beyotime Inc, China). Protein concentration was normalized using the BCA protein assay kit (Thermos, USA). Western blotting was performed by loading 20 μg proteins in each lane on 7.5%, 10% and 12% SDS-PAGE gels (Bio-rad laboratories, USA). Nonspecific binding sites of the nitrocellulose membrane were blocked using 5% skinned milk (BD, MD, USA). After immunoblotting with primary and secondary antibody, the blots were imaged using the ChemiDoc Imaging System (Bio-Rad, Hercules, California, USA). Primary antibodies include rabbit anti-pFAK^Try397 and FAK (Cell Signaling Technology), rabbit anti-cleaved caspase3 (Abcam, Cambridge, MA USA), rabbit anti-IGFBP2 (Proteintech), rabbit anti-ITGA5 (Proteintech) and mouse anti-β actin (Proteintech).

Assessment of mitochondrial membrane potential

Mitochondrial membrane potential was assessed by JC-1 fluorescence dye (beyotine, C2006, China). After treatment, podocytes were incubated with 0.5 mL JC-1 and 0.5 mL complete culture medium at a 37 °C and 5% CO_2 humidified

incubator for 20 min, washed twice by PBS and resuspended in 1 ml of fresh culture medium before measured by Confocal Laser Scanning Microscope (FV3000, Olympus, Japan). The maximal absorption/emission of aggregated red form is 601/620 nm. The maximal absorption/emission of monomeric green form is 529/540 nm.

Measuring mtSOX and ROS production

Briefly, after different treatments, podocyte was harvested and incubated with 20 mM mitochondrial superoxide (mtSOX) detection dye (MT14, Dojindo, Japan) in serum-free medium for 30 min, or 5 mM 5-(and-6)-chloromethyl-2′,7′-dichlorodihydrofluorescein diacetate, acetyl ester mixed isomers (C6827, Invitrogen) in serum-free medium for 40 min at 37℃ in the dark. After incubation, samples were washed twice with cold PBS, then reveled by Confocal Laser Scanning Microscope (FV3000, Olympus, Japan) (mtSOX: Ex at 661 nm, Em at 650–750 nm; ROS: Ex at 517 nm, Em at 517-527 nm), and analyzed using Image J software.

Annexin V/PI apoptosis assay

Annexin V-FITC/PI was obtained from Dojindo. Podocytes were collected and incubated with 5 μl Annexin V and 5 μl PI solution at room temperature for 15 min in the dark. Cellular apoptosis was detected with flow cytometry at an excitation wavelength of 488 nm. FITC fluorescence was detected at a wavelength of 515 nm, and PI was detected at a wavelength of 560 nm.

Co-immunoprecipitation (CO-IP) assays

According to standard protocols, 293T cell transfected with IGFBP2-Flag, ITGA5-Myc, Vehicle-Myc or Vehicle-Flag with HG 48 stimulation were scraped off directly with a cell scraper using immunoprecipitation lysis buffer containing 1 mM PMSF and protease inhibitor. Then, cell was centrifuged at $12,000 \times$ rpm for 15 min at 4 °C, and the supernatant was collected, followed by incubation with anti-IGFBP2 or anti-ITGA5 gentle rocking overnight at 4 °C. The next day, protein A/G beads (#sc-2003, Santa cruz, Shanghai, China) was added to each immunoprecipitation mixture with gentle rocking 4 h at 4 °C. Then, the mixtures were washed five times with cold RIPA with PMSF, and bound protein was denatured with $2 \times$ SDS sample buffer. The supernatants were collected and proceeded to SDS-PAGE Western blotting analysis.

Statistical analysis

All data were expressed as the mean $\pm$ SD or SEM. Statistically significant differences were defined as $P < 0.05$. Statistical analyses were perform using SPSS Statistics 26.0 software (version 26.0, SPSS, Chicago, IL, USA) and GraphPad Prism software (Vision 9.5, San Diego, CA, USA).

Result

IGFBP2 is increased in DKD patients, mouse and podocyte

Morning urinary sample from patients with diabetes mellitus (DM) and diabetic kidney disease (DKD) was collected for ELISA test. There were no significant differences between gender and age in DM and DKD group. Urinary IGFBP2 level was significantly higher among DKD participants in comparison with DM group (Fig. 1A). We further measured IGFBP2 mRNA expression in the STZ-induced DN mice and found it was also highly expressed compared with that in healthy mice (Fig. 1B). IGFBP2 protein level was also expressed at significantly higher in STZ-induced DKD mice than that in healthy mice (Fig. 1C-D). Furthermore, we examined the IGFBP2 mRNA and protein expression under the culture of normal glucose (NG, 5 mM) or high glucose (HG, 30 mM) with different time points of 24, 48 and 72 h on human podocyte. As shown in Fig. 1E–G, podocyte exposure to HG showed an elevation of IGFBP2 mRNA and protein expression in time dependent way, significantly increasing in HG48h and 72 h. These results suggest the expression of IGFBP2 was increased in diabetic environment, supporting our hypothesis that the possible correlation between IGFBP2 and DKD procession.

IGFBP2^{null} mouse retards diabetes-associated glomerulopathy on podocyte

To explore the role of which IGFBP2 induces DKD development, we studied DKD development in IGFBP2^{null} mouse. As shown in Fig. 2A, the STZ (50 mg/kg for 5d) or citrate buffer intraperitoneal injection were performed on 8-week-old IGFBP2^{wt} and IGFBP2^{null} mouse, and all mouse were euthanized at 16 weeks after STZ induction. Although IGFBP2 deficiency virtually decreased the albumin-to-creatine ratio of random urine sample in diabetic IGFBP2^{null} mouse compared with those in diabetic IGFBP2^{wt} mouse after 16-week treatment, it did not significantly affect body weight, and blood glucose between diabetic IGFBP2^{wt} and IGFBP2^{null} mouse as well as non-diabetic mouse (Fig. 2B-C). However, in the diabetic IGFBP2^{null} mouse, the STZ-induced kidney hypertrophy shown by kidney-to-body weight ratio decreased more than those in diabetic IGFBP2^{wt} mice (Fig. 2D). In the case of albuminuria levels, the albumin-to-creatinine ratio (ACR) of random urine samples was similar to those of kidney hypertrophy in diabetic mice

(Fig. 2E). Additionally, in the renal tissue, the glomerular volume and mesangial expansion were markedly attenuated in diabetic IGFBP2^{null} mice compared with diabetic IGFBP2^{wt} mice (Fig. 2F-G). These findings suggest that IGFBP2 deficiency protected elevation of kidney-to-body weight ratio and ACR from STZ induction.

Consistently, we found that significantly reduced number of foot process and obviously thickened GBM were revealed by transmission electron microscopic analysis in diabetic IGFBP2^{wt} mice, while those were alleviated in diabetic IGFBP2^{null} mice (Fig. 3A-C). We evaluated glomerular apoptosis in diabetic IGFBP2^{wt} and IGFBP2^{null} mouse as

well as non-diabetic mouse by terminal deoxynucleotidyl transferase dUTP nick end labeling (TUNEL) staining, which showed a significant reduction in the number of glomerular cells diabetic IGFBP2^{null} mice (Fig. 3D-E). In contrast, a significant increase in TUNEL/DAPI of glomerular cells in diabetic IGFBP2^{wt} mice was observed in comparison with non-diabetic IGFBP2^{wt} mice. The single cell analysis data from public database shows that IGFBP2 is mainly located in podocyte. Thus, we subsequently support the location of IGFBP2 on podocyte shown by immunofluorescent stain (Fig. 3F). Besides that, WT1 staining result confirmed deficiency of IGFBP2 could alleviate the decreasing number
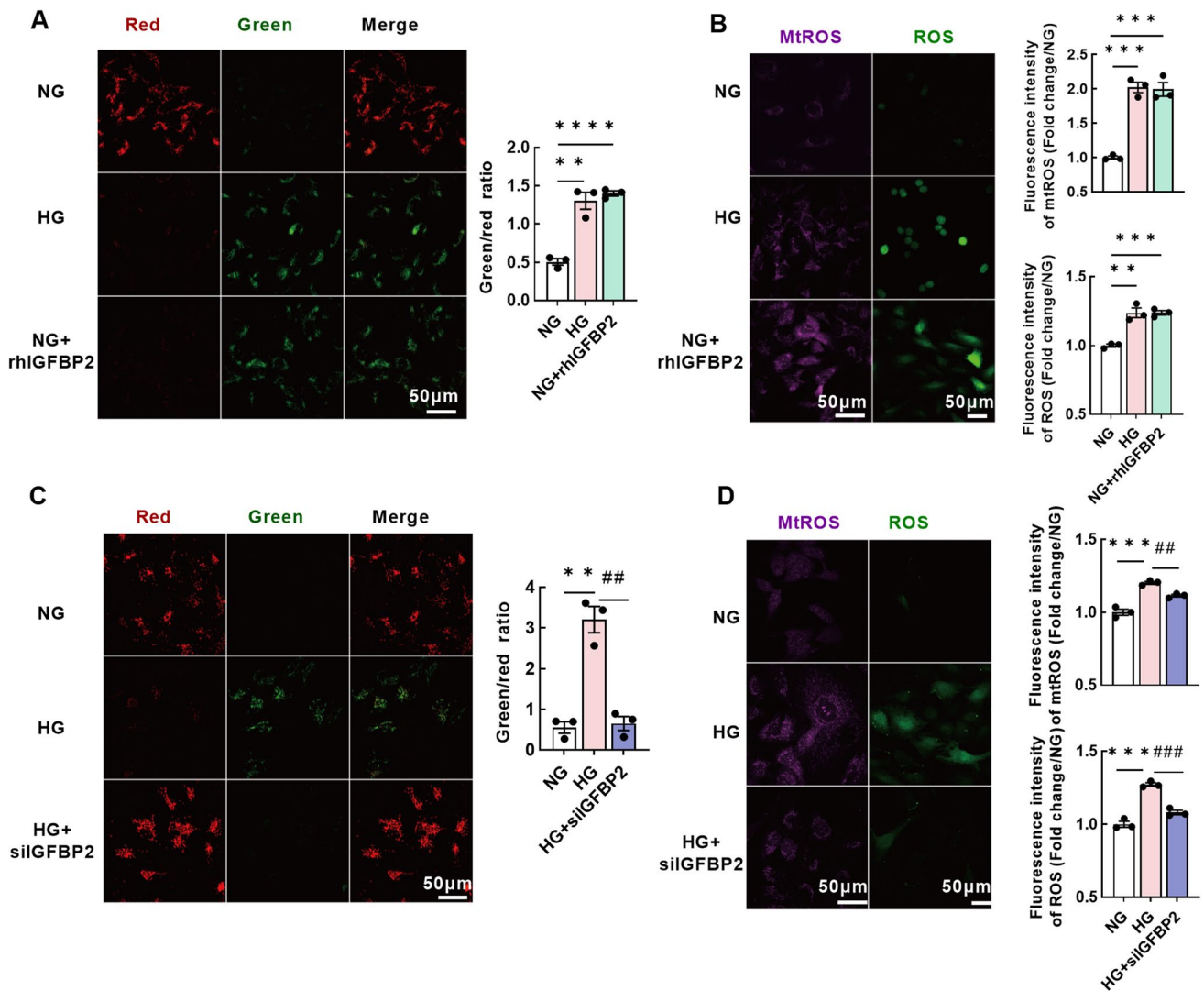

Fig. 5 IGFBP2 regulates mitochondrial damage induced oxidative stress on podocyte. **A** Representative images and quantification of mitochondrial membrane potentials on podocyte under NG, HG and NG with 125 ng/ml rhIGFBP2 treatments. Scale bars = 50 μm. **B** Representative images and quantification of mtROS detected by MitoSOX Deep Red and cellular ROS detected by CM-H2DCFDA on podocyte under NG, HG and NG with 125 ng/ml rhIGFBP2 treatments. Scale bars = 50 μm. **C** Representative images and quantification of mitochondrial membrane potentials on podocyte under NG, HG and HG with siIGFBP2 conditions. Scale bars = 50 μm. **D** Representative images and quantification of mtROS and cellular ROS on podocyte under NG, HG and HG with siIGFBP2 conditions. Scale bars = 50 μm. All data shown as mean ± SEM. **$P < 0.01$, ***$P < 0.001$, ****$P < 0.0001$; ##$P < 0.01$, ###$P < 0.001$
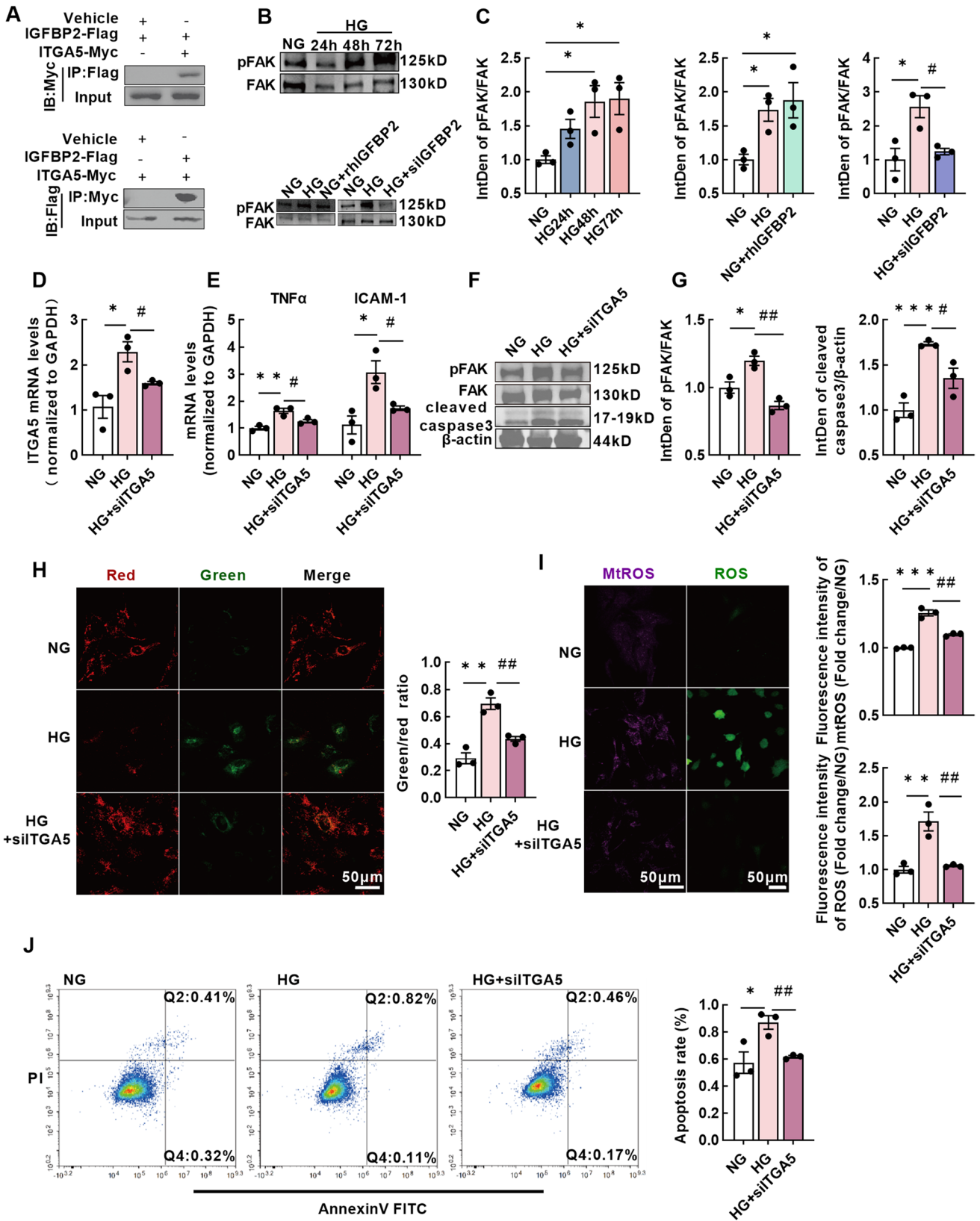
◄**Fig. 6** IGFBP2 regulates the mitochondrial induced podocyte apoptosis by ITGA5/FAK signaling. **A** Potential interaction between IGFBP2 and ITGA5 on 293T cell surface performed by Co-immunoprecipitation analysis. **B**, **C** Representative images and quantification of pFAK/FAK detected by western blot on podocyte under NG, HG, NG with 125 ng/ml rhIGFBP2 and HG with siIGFBP2 conditions. n = 3. **D** Transfection efficiency of IGFBP2 in podocyte interfered with siITGA5 under HG condition performed by RT-qPCR analysis. n = 3. **E** RT-qPCR analysis of TNF-α and ICAM-1 mRNA expression on podocyte under NG, HG and HG with siITGA5 conditions. n = 3. **F**, **G** Representative images and quantification of pFAK/FAK and cleaved caspase3 detected by western blot on podocyte under NG, HG, and HG with siITGA5 conditions. n = 3. **H** Representative images and quantification of mitochondrial membrane potentials on podocyte under NG, HG, and HG with siITGA5 conditions. n = 3. **I** Representative images and quantification of mtROS detected by MitoSOX Deep Red and cellular ROS detected by CM-H2DCFDA on podocyte under NG, HG, and HG with siITGA5 conditions. Scale bars = 50 μm. **J** Representative graphs and quantification of apoptosis rate on podocyte performed by flow cytometry under NG, HG and HG with siITGA5 conditions. n = 3. All data shown as mean ± SEM. $^*P < 0.05$, $^{**}P < 0.01$, $^{***}P < 0.001$; $^#P < 0.05$, $^{##}P < 0.01$

of podocytes on diabetic glomeruli (Fig. 3F-G). These findings suggest that IGFBP2 deficiency protected podocyte from STZ-induced diabetic injury and delayed the DKD progression in a great extent. To find the relationship of IGFBP2 with podocyte in DKD process, we assessed mRNA and protein expression of proinflammatory factor and cleaved caspase3 in mice. As expected, the mRNA expression of TNFα and ICAM-1 significantly increased in diabetic mice, while the inflammatory response was attenuated in diabetic IGFBP2^{null} mice (Fig. 3H). Consistent with this finding, we confirmed protein expression of cleaved caspase 3 elevated in diabetic IGFBP2^{wt} mouse after 16 weeks STZ injection, while this elevation was weakened in diabetic IGFBP2^{null} mice (Fig. 3I-J). Together with, IGFBP2 promotes the development and progression of DKD by its possible effect on inflammation and apoptosis and prevents diabetic induced podocyte injury by IGFBP2 inhibition.

IGFBP2 knockdown reduces renal inflammation and apoptosis on podocyte

To verify the potential effect of IGFBP2 on podocyte under in vitro high glucose stimulation, we first tested mRNA expression of TNFα and ICAM-1, as well as the protein levels of cleaved-caspase3 with different time of HG stimulation. Consistent with change of IGFBP2 on podocyte, we found a time dependent increase of TNFα and ICAM-1 using RT-qPCR analysis, significantly elevation at HG 48 h and 72 h (Fig. 4A). Similarly, western blotting result showed that compared with it in NG group, cleaved-caspase3 levels significantly increased in 48 h and 72 h after HG stimulation (Fig. 4B-C). Together with the protein levels of IGFBP2 and cleaved caspase3 as above study shown in podocyte, we picked HG48h in further in vitro exploration.

It is mentioned that IGFBP2 knockdown could be a potential nephroprotective factor, so we silenced IGFBP2 with small interference RNA with lipo3000 package in HG stimulation (Fig. 4D). Fortunately, mRNA expression of TNFα and ICAM-1, and cleaved caspase3 protein level were downregulated remarkably in HG + siIGFBP2 podocyte as detected in mice model (Fig. 4E-H). Moreover, we verified the significantly increased early(Q2) and late(Q4) apoptosis in HG stimulation with comparison to NG stimulation; in contrast, the decreased apoptotic rate in HG + siIGFBP2 podocyte with statistical significance, as measured by the FITC, PI flow cytometry (Fig. 4I-J). To further determine whether podocyte injury could be induced by IGFBP2, recombinant human IGFBP2 (rhIGFBP2, 125 ng/ml) was used to stimulate podocyte. These factors were also increased in NG + 125 ng/ml rhIGFBP2 than those in NG group (Fig. 4K-O). As above, it suggested that IGFBP2 promote cell inflammation by producing proinflammatory factors and activating cleaved-caspase3 in injury podocyte, partially apoptosis could be rescued by siIGFBP2 treatment under HG conditions. However, lack of study discusses the potential mechanism of IGFBP2 on podocyte during DKD process. Our group pervious study has demonstrated that mitochondria damage induced oxidative stress can promote podocyte apoptosis with diabetic induced injury [10]. Therefore, we hypotheses that mitochondrial injury and oxidative stress are the potential linkage between IGFBP2 and podocyte apoptosis.

Thus, to determine whether IGFBP2 levels activate mitochondrial injury and oxidative stress and assess its regulation on podocyte apoptosis, three methods were used on podocytes: fluorescent staining of JC-1, Mito sox and CM-H2DCFDA ROS. When podocytes are healthy, mitochondria form JC-1 polymer with high potential and show red fluorescence; in contrast, mitochondria produce JC-1 monomer with low potential and show green fluorescence, when podocytes are injured. Thus, red to green fluorescence transition indicates cell death and mitochondrial dysfunction. Experiments using the JC-1, Mito sox and ROS staining revealed that NG + 125 ng/ml rhBP2 markedly decreased the mitochondrial membrane potential and promoted mitochondrial superoxide (mtROS) and cellular ROS production on podocyte, compared with NG group (Fig. 5A-B). Furthermore, we compared levels of mitochondrial damage treated with NG, HG, or HG + siIGFBP2 group. Podocyte treated with the siRNA interfering IGFBP2 had increased mitochondrial potential, decreased fluorescent intensity of mtROS, cellular ROS compared to podocyte treated with HG (Fig. 5C-D). In contrast, there was no significant difference in mtROS, cell ROS and apoptosis between cells treated with NG and HG transfected with siIGFBP2. Together, our results suggest that IGFBP2 has a possible effect on regulation of podocyte apoptosis through mitochondrial damage, as hypothesized previously.

IGFBP2 induces mitochondrial injury and oxidative stress through ITGA5/FAK phosphorylation pathway

As previous studies supported, IGFBP2 could bind integrin to regulate cell process [28, 29]. However, there is no evidence to prove whether it happens on podocyte apoptosis in DKD progress. Therefore, we prepared co-immunoprecipitation to determine if IGFBP2 bound to the 293T cell surface, and the result revealed IGFBP2 and ITGA5 could be reaction with each other (Fig. 6A). Furthermore, since ITGA5 could regulate apoptosis via FAK phosphorylation signaling [30], we firstly detected ratio of pFAK/FAK in NG, HG, NG + 125 ng/ml rhIGFBP2 and HG + siIGFBP2 group. Western blot analyses showed a gradual increase in FAK phosphorylation at Try397 with time during HG stimulation, which was similar with increase in cleaved caspase 3. The ratio of pFAK/FAK was increased in HG with different time points compared to NG group via western blot analysis, with significant increase in HG48h and HG72h (Fig. 6B-C). Likewise, podocyte was also stimulated to activate FAK phosphorylation in response to 125 ng/ml rhIGFBP2 stimulus under NG environment (Fig. 6B-C). Additionally, podocyte treated with the siRNA interfering IGFBP2 decreased FAK phosphorylation demonstrated by western blot (Fig. 6B-C).

To fully understand the signal mechanism between ITGA5/FAK, mitochondrial injury, oxidative stress and apoptosis, we used above methods to measure FAK phosphorylation, mitochondrial membrane potential, mtROS, cellular ROS, proinflammation factor mRNA expression and apoptosis on podocyte treated with NG, HG, HG + siITGA5 or HG + PND-1186 (0.4 µM, FAK inhibitor). The siITGA5 treatment exerted a significantly effect of inhibition of FAK phosphorylation, elevation of mitochondrial membrane potential and reduction of mtROS, cellular ROS, proinflammatory factors, and apoptosis in HG + siITGA5 group (Fig. 6D-J). Thus, FAK phosphorylation could be regulated after IGFBP2 binding to ITGA5. Likewise, 0.4 µM PND-1186 significantly alleviated HG-induced mitochondrial depolarization, oxidative stress, inflammation, and apoptosis (Fig. 7A-F).

To further confirm the mechanism by which IGFBP2 regulates podocyte apoptosis via ITGA5/FAK signaling, we transfected with IGFBP2 overexpression (IGFBP2^{OV}) vehicle with following treatment of siITGA5 or 0.4 µM PND-1186. Similar with rhIGFBP2 stimulus, IGFBP2^{OV} could significantly increase podocyte apoptosis via FAK phosphorylation, mtROS, cellular ROS and proinflammatory factors (Fig. 8). Corresponding with earlier experiment, p-FAK/FAK was significantly downregulated after podocyte in treatment with siITGA5 and PND-1186 (Fig. 8B-E). Moreover, siITGA5 and PND-1186 treatment showed the elevation of mitochondria membrane potential and inhibition of mtROS and cellular ROS, TNFα, ICAM-1, and cleaved caspase3 at 48 h post IGFBP2^{OV} transfection compared with

these in IGFBP2^{OV} group (Fig. 8B-K). In vivo study, western blot analysis also showed a decrease in FAK phosphorylation at diabetic IGFBP2^{null} mice than those at diabetic IGFBP2^{wt} mice (Fig. 8L). Taken together, our results provide mechanistic evidence that podocyte apoptosis could be reduced by inhibiting the levels of IGFBP2, ITGA5, FAK with PND-1186 during HG stimulation. These indicates that IGFBP2 induce podocyte inflammation and apoptosis by mtROS and cellular ROS through ITGA5/FAK.

Discussion

Interest in podocyte apoptosis as a source for diabetic kidney disease (DKD) has been widely reported [31, 32], but there is still lack of specifically target to treat. Here, we found that, 1) IGFBP2 is highly secreted in urine from DKD patients, 2) IGFBP2 promotes mitochondrial damage, oxidative stress, and inflammation of human podocyte under hyperglycemia, 3) the apoptosis of IGFBP2 on human podocytes depends on ITGA5/FAK/ROS signaling, and 4) inhibition of IGFBP2 alleviates renal damage in vivo and vitro experiment of DKD. IGFBP2 is therefore a target damage factor of apoptosis in hyperglycemia renal injury. These observations highlight the importance of the IGFBP2/ITGA5/FAK axis in overcoming mitochondrial damage, oxidative stress, inflammation and apoptosis suggest that IGFBP2 knockdown and FAK dephosphorylation provides a theoretical basis for the design of treatment options and targeted drugs.

Although pervious reports showed the potential association between IGFBP2 and diabetes mellites, most of these studies focused on circulating IGFBP2 as an effector and few focused on its effect on glomerulus in DKD [18, 33]. Despite of antidiabetic effect of IGFBP2 by improved leptin sensitivity of diabetic mouse model [34], our results showed that deleting IGFBP2 had a downward trend in diabetic mice without statistical significance. Consistent with findings in these diabetic patients with proteinuria [35], our results showed that IGFBP2 where it could be expressed and secreted by podocytes, was found to significantly increased in urine sample with DKD patients. Moreover, inflammation is a crucial step of cell apoptosis and has been shown to be regulated by IGFBP2 [20]. Our results also indicated that elevation of TNFα and ICAM-1 level in podocyte contributed to apoptosis that could be alleviated by IGFBP2 knockdown. Other research showed that inflammation could increase IGFBP2 level with elevation of cleaved caspase3 [19], which indicated that inflammation could positively feedback to promote IGFBP2 in cell death process. However, we only discuss the regulation effect of IGFBP2 on proinflammatory factor rather than their communication in podocyte apoptosis. Thus, further research can focus on the feedback mechanism of which proinflammatory factors and IGFBP2 expression.
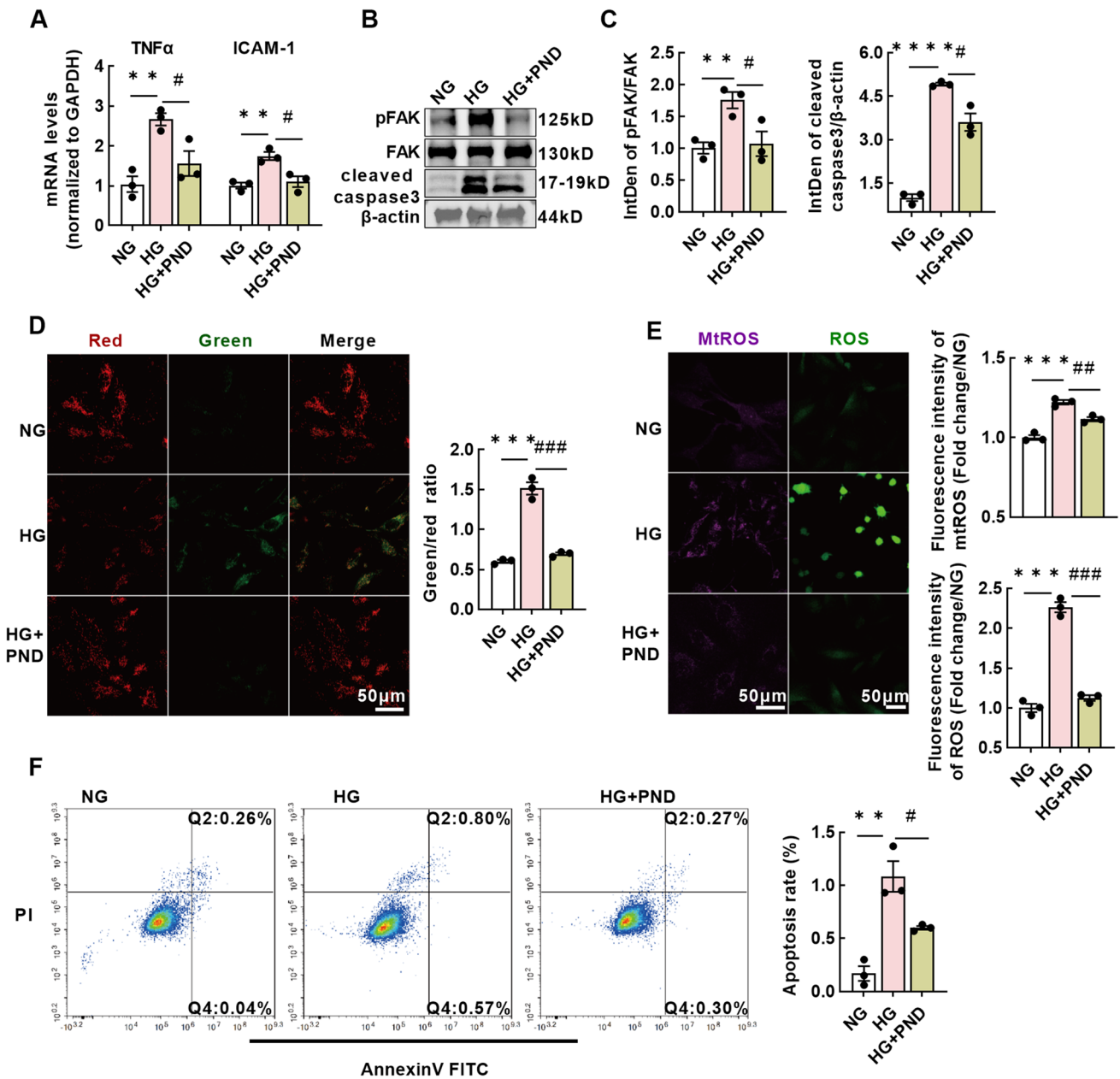
Fig. 7 Inhibition of FAK phosphorylation alleviates mitochondrial induced oxidative stress and podocyte apoptosis. **A** RT-qPCR analysis of TNF-α and ICAM-1 mRNA expression on podocyte under NG, HG and HG with 0.4 μM PND-1186(FAK inhibitor) conditions. n = 3. **B, C** Representative images and quantification of pFAK/FAK and cleaved caspase3 detected by western blot on podocyte under NG, HG and HG with 0.4 μM PND-1186. n = 3. **D** Representative images and quantification of mitochondrial membrane potentials on podocyte under NG, HG and HG with 0.4 μM PND-1186. n = 3. **E** Representative images and quantification of mtROS detected by MitoSOX Deep Red and cellular ROS detected by CM-H2DCFDA on podocyte under NG, HG and HG with 0.4 μM PND-1186. Scale bars = 50 μm. **F** Representative graphs and quantification of apoptosis rate on podocyte performed by flow cytometry under NG, HG and HG with 0.4 μM PND-1186. n = 3. All data shown as mean ± SEM. **$P < 0.01$, ***$P < 0.001$, ****$P < 0.0001$; #$P < 0.05$, ##$P < 0.01$, ###$P < 0.001$

Several researches have shown that mitochondrial injury induced oxidative stress is a prominent feature of podocyte apoptosis during the procession of DKD [10, 36]. Mitochondrial injury induced oxidative stress is association with secretion of proinflammatory factors such as TNFα and ICAM-1 in DKD [37, 38]. Together with these, diabetes models have shown oxidative stress in podocyte and inhibiting mitochondrial injury can revert podocyte loss and proteinuria [37, 39]. Mitochondrial injury increases ROS accumulation and apoptotic protein secretion, all of which
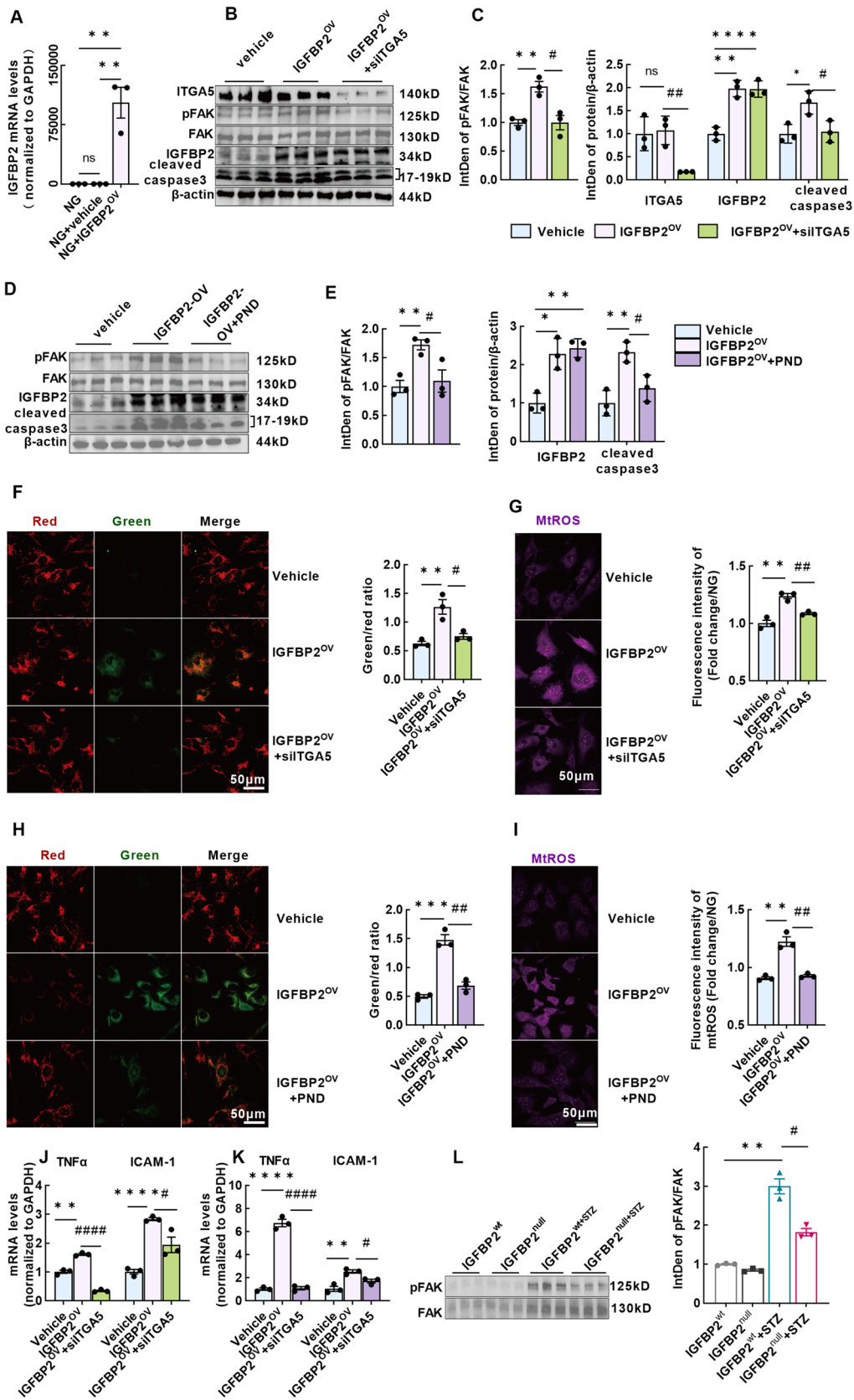
◄**Fig. 8** Inhibition of ITGA5 and pFAK alleviates IGFBP2-mediated podocyte apoptosis by reducing mitochondrial induced oxidative stress. **A** Expression of IGFBP2 mRNA in IGFBP2^{ov} human podocyte compared with the NG and NG with vehicle conditions. n = 3. **B**, **C** Representative images and quantification of pFAK/FAK, ITGA5, IGFBP2 and cleaved caspase3 detected by western blot in IGFBP2^{ov}, IGFBP2^{ov} with siITGA5 and vehicle podocyte under NG conditions. n = 3. **D**, **E** Representative images and quantification of pFAK/FAK, IGFBP2 and cleaved caspase3 detected by western blot in IGFBP2^{ov}, IGFBP2^{ov} with 0.4 μM PND-1186 and vehicle podocyte under NG conditions. **F** Representative images and quantification of mitochondrial membrane potentials in IGFBP2^{ov}, IGFBP2^{ov} with siITGA5 and vehicle podocyte under NG conditions. Scale bars = 50 μm. **G** Representative images and quantification of mtROS detected by MitoSOX Deep Red in IGFBP2^{ov}, IGFBP2^{ov} with siITGA5 and vehicle podocyte under NG conditions. Scale bars = 50 μm. **H** Representative images and quantification of mitochondrial membrane potentials in IGFBP2^{ov}, IGFBP2^{ov} with 0.4 μM PND-1186 and vehicle podocyte under NG conditions. Scale bars = 50 μm. **I** Representative images and quantification of mtROS detected in IGFBP2^{ov}, IGFBP2^{ov} with 0.4 μM PND-1186 and vehicle podocyte under NG conditions. Scale bars = 50 μm. **J** RT-qPCR analysis of TNF-α and ICAM-1 mRNA expression in IGFBP2^{ov}, IGFBP2^{ov} with siITGA5 and vehicle podocyte under NG conditions. **K** RT-qPCR analysis of TNF-α and ICAM-1 mRNA expression in IGFBP2^{ov}, IGFBP2^{ov} with 0.4 μM PND-1186 and vehicle podocyte under NG conditions. **L** Representative images and quantification of pFAK/FAK detected by western blot in diabetic and non-diabetic IGFBP2^{wt} and IGFBP2^{null} mice. All data shown as mean ± SEM. n = 3 **$P < 0.01$, ***$P < 0.001$, ****$P < 0.0001$; #$P < 0.05$, ##$P < 0.01$, ####$P < 0.0001$

aggravate podocyte apoptosis and promote DKD progress [10, 40]. ROS accumulation is the major mechanism of podocyte apoptosis during the HG stimulation and mainly secreted by mitochondria [37]. Our previous study has shown that ginsenoside Rb1 can be used to alleviate podocyte apoptosis and detachment, and to reduce ROS overproduction by inhibiting HG-induced mitochondrial damage [10]. Thus, mitochondrial injury could be a potential way to maintain the balance of oxidation and anti-oxidation. Our results showed that IGFBP2 promoted mitochondrial injury and further increased level of cellular oxidant on podocyte. After endogenous or exogenous IGFBP2 stimulation, mitochondrial injury was found to increase with ROS accumulation and inflammation, which could be alleviated after knocking down IGFBP2.

Further exploring IGFBP-2 signaling responses in podocyte, we found an increase in active ITGA5 by HG stimulation, but no difference following endogenous IGFBP2 treatment. Interestingly, IGFBP2 contains an RGD domain (CGGGGGGAC) that can bind to ITGA5 via IGF independent pathway [41]. Studies have shown that high expression of ITGA5 resulting from glucose is involved in the pathological changes such as mesangial expansion and thicken of the basement membrane in DKD [42, 43]. In line with other cells, the effect of IGFBP2 on cell mobility have been attributed to the modulation of ITGA5/FAK [21, 24]. Many studies have shown that FAK-mediated mitochondrial

apoptotic injury regulates ROS production [26, 44]. In tumor-associated macrophages, integrin/FAK phosphorylation induce increasing mitochondrial ROS production by reducing SIRT3 signal transduction [26]. In addition, increased FAK-mediated ROS and enhanced apoptosis can also be observed in diabetic cardiomyocytes [44]. Moreover, there is also evidence that decreased FAK activity occurs in diabetic podocyte injury, with increasing podocyte adhesion protect against early DKD in vitro and vivo study. However, this study showed the f-actin loss with high expression of p-FAK, and previous study has demonstrated the apoptotic effect of f-actin loss on podocyte [13]. Therefore, in part at least, FAK phosphorylation could be a detrimental factor referring to its function on mitochondrial oxidative stress and loss of cell skeleton. Podocyte apoptosis has been also reported to be associated with integrin/FAK signaling [45]. Our data showed that FAK phosphorylation was elevated in DKD and increased mitochondrial injury, ROS production and apoptosis in podocyte. ITGA5 knockdown and inhibition of FAK phosphorylation not only reversed the increase in mitochondrial ROS production but also alleviated podocyte inflammation and apoptosis.

Inhibiting of ITGA5/FAK signaling blocked the effects of mitochondrial ROS on podocyte associated with IGFBP2. Our result showed the regulating oxidative stress could be a treatment to protect against podocyte apoptosis. Future studies using podocyte-specific IGFBP2 knockout or other glomerular diseases mouse model are suggested to fully understand the role of IGFBP2 on podocyte apoptosis. Concordant with previous studies, IGFBP2 is discovered to be a possible prognostic biomarker in diabetic patients with elevation of albuminuria and reduction of GFR. Also, of note, we only discuss the effects of IGFBP2 on podocyte apoptosis via ITGA5/FAK/ROS signaling without its function on cell skeleton. Further studies are needed to explore the detailed mechanism by which IGFBP2 promoted podocyte injury in glomerular diseases and confirmed its potential therapeutical function.

In summary, we demonstrated that IGFBP2 regulated podocyte apoptosis via ITGA5/FAK/ROS signaling pathway in DKD progression. A significant elevation in IGFBP2 in STZ-induced DKD, where it is expressed by podocytes and activated proinflammatory factors secretion, facilitates mitochondrial-mediated oxidative injury via FAK phosphorylation. IGFBP2 knockdown blunted the possible apoptotic effect of podocyte in DKD. Thus, strategies to silence IGFBP2 levels in diabetes could protect podocyte function.

Data availability No datasets were generated or analysed during the current study.

Declarations

Competing interests The authors declare no competing interests.

References

1. Kato M, Natarajan R (2019) Epigenetics and epigenomics in diabetic kidney disease and metabolic memory. Nat Rev Nephrol 15(6):327–345

2. Cleveland KH, Schnellmann RG (2023) Pharmacological targeting of mitochondria in diabetic kidney disease. Pharmacol Rev 75(2):250–262

3. Tuttle KR, Agarwal R, Alpers CE, Bakris GL, Brosius FC, Kolkhof P, Uribarri J (2022) Molecular mechanisms and therapeutic targets for diabetic kidney disease. Kidney Int 102(2):248–260

4. Vartak T, Godson C, Brennan E (2021) Therapeutic potential of pro-resolving mediators in diabetic kidney disease. Adv Drug Deliv Rev 178:113965

5. Chen Z, Zhu Z, Liang W, Luo Z, Hu J, Feng J, Zhang Z, Luo Q, Yang H, Ding G (2023) Reduction of anaerobic glycolysis contributes to angiotensin II-induced podocyte injury with foot process effacement. Kidney Int 103(4):735–748

6. Pagtalunan ME, Miller PL, Jumping-Eagle S, Nelson RG, Myers BD, Rennke HG, Coplon NS, Sun L, Meyer TW (1997) Podocyte loss and progressive glomerular injury in type II diabetes. J Clin Invest 99(2):342–348

7. Toyoda M, Najafian B, Kim Y, Caramori ML, Mauer M (2007) Podocyte detachment and reduced glomerular capillary endothelial fenestration in human type 1 diabetic nephropathy. Diabetes 56(8):2155–2160

8. Song S, Shi C, Bian Y, Yang Z, Mu L, Wu H, Duan H, Shi Y (2022) Sestrin2 remedies podocyte injury via orchestrating TSP-1/TGF-β1/Smad3 axis in diabetic kidney disease. Cell Death Dis 13(7):663

9. Xu S, Nam SM, Kim JH, Das R, Choi SK, Nguyen TT, Quan X, Choi SJ, Chung CH, Lee EY et al (2015) Palmitate induces ER calcium depletion and apoptosis in mouse podocytes subsequent to mitochondrial oxidative stress. Cell Death Dis 6(11):e1976

10. He JY, Hong Q, Chen BX, Cui SY, Liu R, Cai GY, Guo J, Chen XM (2022) Ginsenoside Rb1 alleviates diabetic kidney podocyte injury by inhibiting aldose reductase activity. Acta Pharmacol Sin 43(2):342–353

11. Doublier S, Seurin D, Fouqueray B, Verpont MC, Callard P, Striker LJ, Striker GE, Binoux M, Baud L (2000) Glomerulosclerosis in mice transgenic for human insulin-like growth factor-binding protein-1. Kidney Int 57(6):2299–2307

12. Yu JT, Hu XW, Yang Q, Shan RR, Zhang Y, Dong ZH, Li HD, Wang JN, Li C, Xie SS et al (2022) Insulin-like growth factor binding protein 7 promotes acute kidney injury by

13. alleviating poly ADP ribose polymerase 1 degradation. Kidney Int 102(4):828–844

14. Lay AC, Hale LJ, Stowell-Connolly H, Pope RJP, Nair V, Ju W, Marquez E, Rollason R, Hurcombe JA, Hayes B et al (2021) IGFBP-1 expression is reduced in human type 2 diabetic glomeruli and modulates β1-integrin/FAK signalling in human podocytes. Diabetologia 64(7):1690–1702

15. Park IS, Kiyomoto H, Alvarez F, Xu YC, Abboud HE, Abboud SL (1998) Preferential expression of insulin-like growth factor binding proteins-1, -3, and -5 during early diabetic renal hypertrophy in rats. Am J Kidney Dis 32(6):1000–1010

16. AlMajed HT, Abu-Farha M, Alshawaf E, Devarajan S, Alsairafi Z, Elhelaly A, Cherian P, Al-Khairi I, Ali H, Jose RM et al (2023) Increased levels of circulating IGFBP4 and ANGPTL8 with a prospective role in diabetic nephropathy. Int J Mol Sci 24(18):14244

17. Song C, Wang S, Fu Z, Chi K, Geng X, Liu C, Cai G, Chen X, Wu D, Hong Q (2022) IGFBP5 promotes diabetic kidney disease progression by enhancing PFKFB3-mediated endothelial glycolysis. Cell Death Dis 13(4):340

18. Li T, Forbes ME, Fuller GN, Li J, Yang X, Zhang W (2020) IGFBP2: integrative hub of developmental and oncogenic signaling network. Oncogene 39(11):2243–2257

19. Faramia J, Hao Z, Mumphrey MB, Townsend RL, Miard S, Carreau AM, Nadeau M, Frisch F, Baraboi ED, Grenier-Larouche T et al (2021) IGFBP-2 partly mediates the early metabolic improvements caused by bariatric surgery. Cell Rep Med 2(4):100248

20. Chiu YJ, Lee CM, Lin TH, Lin HY, Lee SY, Mesri M, Chang KH, Lin JY, Lee-Chen GJ, Chen CM (2018) Chinese herbal medicine glycyrrhiza inflatareduces Aβ aggregation and exerts neuroprotection through anti-oxidation and anti-inflammation. Am J Chin Med 46(07):1535–1559

21. Zhang J, Jin L, Hua X, Wang M, Wang J, Xu X, Liu H, Qiu H, Sun H, Dong T et al (2023) SARM1 promotes the neuroinflammation and demyelination through IGFBP2/NF-κB pathway in experimental autoimmune encephalomyelitis mice. Acta Physiol (Oxf) 238(2):e13974

22. Wang GK, Hu L, Fuller GN, Zhang W (2006) An interaction between insulin-like growth factor-binding protein 2 (IGFBP2) and integrin alpha5 is essential for IGFBP2-induced cell mobility. J Biol Chem 281(20):14085–14091

23. Narayanan RP, Fu B, Heald AH, Siddals KW, Oliver RL, Hudson JE, Payton A, Anderson SG, White A, Ollier WE et al (2012) IGFBP2 is a biomarker for predicting longitudinal deterioration in renal function in type 2 diabetes. Endocr Connect 1(2):95–102

24. Firth SM, Baxter RC (2002) Cellular actions of the insulin-like growth factor binding proteins. Endocr Rev 23(6):824–854

25. Liu Y, Li F, Yang YT, Xu XD, Chen JS, Chen TL, Chen HJ, Zhu YB, Lin JY, Li Y et al (2019) IGFBP2 promotes vasculogenic mimicry formation via regulating CD144 and MMP2 expression in glioma. Oncogene 38(11):1815–1831

26. Ma H, Togawa A, Soda K, Zhang J, Lee S, Ma M, Yu Z, Ardito T, Czyzyk J, Diggs L et al (2010) Inhibition of podocyte FAK protects against proteinuria and foot process effacement. J Am Soc Nephrol 21(7):1145–1156

27. Liu X, Hogg GD, Zuo C, Borcherding NC, Baer JM, Lander VE, Kang LI, Knolhoff BL, Ahmad F, Osterhout RE et al (2023) Context-dependent activation of STING-interferon signaling by CD11b agonists enhances anti-tumor immunity. Cancer Cell 41(6):1073-1090.e1012

28. Hotta N, Akanuma Y, Kawamori R, Matsuoka K, Oka Y, Shichiri M, Toyota T, Nakashima M, Yoshimura I, Sakamoto N et al (2006) Long-term clinical effects of epalrestat, an aldose reductase inhibitor, on diabetic peripheral neuropathy: the 3-year, multicenter, comparative aldose reductase inhibitor-diabetes complications trial. Diabetes Care 29(7):1538–1544

28. Holmes KM, Annala M, Chua CY, Dunlap SM, Liu Y, Hugen N, Moore LM, Cogdell D, Hu L, Nykter M et al (2012) Insulin-like growth factor-binding protein 2-driven glioma progression is prevented by blocking a clinically significant integrin, integrin-linked kinase, and NF-κB network. Proc Natl Acad Sci U S A 109(9):3475–3480

29. Patil SS, Gokulnath P, Bashir M, Shwetha SD, Jaiswal J, Shastry AH, Arimappamagan A, Santosh V, Kondaiah P (2016) Insulin-like growth factor binding protein-2 regulates β-catenin signaling pathway in glioma cells and contributes to poor patient prognosis. Neuro Oncol 18(11):1487–1497

30. Zhang C, Yu Z, Yang S, Liu Y, Song J, Mao J, Li M, Zhao Y (2024) ZNF460-mediated circRPPH1 promotes TNBC progression through ITGA5-induced FAK/PI3K/AKT activation in a ceRNA manner. Mol Cancer 23(1):33

31. Luna-Sanchez M, Benincá C, Cerutti R, Brea-Calvo G, Yeates A, Scorrano L, Zeviani M, Viscomi C (2020) Opa1 overexpression protects from early-onset Mpv17(-/-)-related mouse kidney disease. Mol Ther 28(8):1918–1930

32. Burlaka I, Nilsson LM, Scott L, Holtbäck U, Eklöf AC, Fogo AB, Brismar H, Aperia A (2016) Prevention of apoptosis averts glomerular tubular disconnection and podocyte loss in proteinuric kidney disease. Kidney Int 90(1):135–148

33. Dreyfuss JM, Yuchi Y, Dong X, Efthymiou V, Pan H, Simonson DC, Vernon A, Halperin F, Aryal P, Konkar A et al (2021) High-throughput mediation analysis of human proteome and metabolome identifies mediators of post-bariatric surgical diabetes control. Nat Commun 12(1):6951

34. Hedbacker K, Birsoy K, Wysocki RW, Asilmaz E, Ahima RS, Farooqi IS, Friedman JM (2010) Antidiabetic effects of IGFBP2, a leptin-regulated gene. Cell Metab 11(1):11–22

35. Akinci A, Copeland KC, Garmong A, Clemmons DR (2000) Insulin-like growth factor binding proteins (IGFBPs) in serum and urine and IGFBP-2 protease activity in patients with insulin-dependent diabetes mellitus. Metabolism 49(5):626–633

36. Chen Z, Liang W, Hu J, Zhu Z, Feng J, Ma Y, Yang Q, Ding G (2022) Sirt6 deficiency contributes to mitochondrial fission and oxidative damage in podocytes via ROCK1-Drp1 signalling pathway. Cell Prolif 55(10):e13296

37. Ke G, Chen X, Liao R, Xu L, Zhang L, Zhang H, Kuang S, Du Y, Hu J, Lian Z et al (2021) Receptor activator of NF-κB mediates podocyte injury in diabetic nephropathy. Kidney Int 100(2):377–390

38. Tanase DM, Gosav EM, Anton MI, Floria M, Seritean Isac PN, Hurjui LL, Tarniceriu CC, Costea CF, Ciocoiu M, Rezus C (2022) Oxidative stress and NRF2/KEAP1/ARE pathway in diabetic kidney disease (DKD): new perspectives. Biomolecules 12(9):1227

39. Chen A, Feng Y, Lai H, Ju W, Li Z, Li Y, Wang A, Hong Q, Zhong F, Wei C et al (2020) Soluble RARRES1 induces podocyte apoptosis to promote glomerular disease progression. J Clin Invest 130(10):5523–5535

40. Gong M, Guo Y, Dong H, Wu F, He Q, Gong J, Lu F (2024) Modified Hu-lu-ba-wan protects diabetic glomerular podocytes via promoting PKM2-mediated mitochondrial dynamic homeostasis. Phytomedicine 123:155247

41. Russo VC, Azar WJ, Yau SW, Sabin MA, Werther GA (2015) IGFBP-2: The dark horse in metabolism and cancer. Cytokine Growth Factor Rev 26(3):329–346

42. Aggarwal PK, Veron D, Thomas DB, Siegel D, Moeckel G, Kashgarian M, Tufro A (2015) Semaphorin3a promotes advanced diabetic nephropathy. Diabetes 64(5):1743–1759

43. Zhou X, Zhang J, Haimbach R, Zhu W, Mayer-Ezell R, Garcia-Calvo M, Smith E, Price O, Kan Y, Zycband E et al (2017) An integrin antagonist (MK-0429) decreases proteinuria and renal fibrosis in the ZSF1 rat diabetic nephropathy model. Pharmacol Res Perspect 5(5):e00354

44. Dai L, Xie Y, Zhang W, Zhong X, Wang M, Jiang H, He Z, Liu X, Zeng H, Wang H (2021) Weighted gene co-expression network analysis identifies ANGPTL4 as a key regulator in diabetic cardiomyopathy via FAK/SIRT3/ROS pathway in cardiomyocyte. Front Endocrinol (Lausanne) 12:705154

45. Ni Y, Wang X, Yin X, Li Y, Liu X, Wang H, Liu X, Zhang J, Gao H, Shi B et al (2018) Plectin protects podocytes from adriamycin-induced apoptosis and F-actin cytoskeletal disruption through the integrin α6β4/FAK/p38 MAPK pathway. J Cell Mol Med 22(11):5450–5467